Evidence for upwards but not downwards influence between the troposphere and the wintertime stratosphere

K. Hartig, N. Harnik, and E. Tziperman

Corresponding author: Kara Hartig, kara_hartig@g.harvard.edu

Abstract

Rossby waves of planetary wavenumber 1 and 2 that are excited in the troposphere can propagate upwards into the stratosphere when conditions are right and disrupt the polar stratospheric vortex. It has been suggested that there is also a downward propagation that allows stratospheric vortex disruptions to influence surface weather conditions, which could improve weather forecast lead times. However, the past few decades of work on stratosphere-troposphere teleconnections have been unable to reach a consensus on either the time scale or consequences for weather of upwards and downwards propagation.

In an attempt to identify significant patterns of covariance between the surface and stratosphere without imposing an expected pattern or timescale, we apply Maximum Covariance Analysis (MCA) with a variable time lag between pairs of tropospheric and stratospheric fields. Using over 60 years of ERA5 reanalysis for Northern Hemisphere winters, we apply MCA by calculating the singular value decomposition of the covariance matrix between a variety of surface and stratospheric fields at time lags up to seven weeks in either direction to pick out the patterns corresponding to the largest covariance between the surface and the stratosphere. We find that the greatest covariance occurs when the surface precedes the stratosphere by about one week, with little evidence of ensuing downwards propagation. The dominant mode corresponding to this one-week lag is not quite the Northern Annular Mode, but something else.

1 Introduction

Dynamic variability in the extratropical stratosphere is strongly dominated on the seasonal scale by the formation and breakdown of the stratospheric polar vortex, which forms in the winter hemisphere, and on the sub-seasonal scale by infrequent but dramatic disruptions of that vortex during Sudden Stratospheric Warmings (SSWs, Andrews et al., 1987; Butler et al., 2015; Baldwin et al., 2021). While the upwards influence of the troposphere on the stratosphere is well-established, it has also been suggested that the stratosphere, even with its much lower mass, is in turn capable of substantially influencing surface weather through downwards propagation. But in spite of significant effort, the characteristics and mechanisms of downward propagation are still not completely understood. Our aim is to identify the time scales and spatial patterns that characterize teleconnections, both upwards and downwards, between stratospheric and tropospheric fields using Maximum Covariance Analysis (Bretherton et al., 1992; Perlwitz & Harnik, 2003, 2004).

SSWs are the most dramatic evidence of the *upwards* influence of the surface on the stratosphere. When the eastward zonal wind in the wintertime stratosphere drops below a critical speed, planetary waves of low wavenumber excited in the troposphere can continue to propagate upwards into the stratosphere (Charney & Drazin, 1961). When these waves break and deposit momentum in a wave-mean flow interaction (Matsuno, 1971; McIntyre & Palmer, 1984; Plumb, 2010), they decelerate the polar jet, resulting in a positive feedback that allows more waves to propagate upwards and subsequently break, further decelerating the jet. This wave breaking feedback can lead to an SSW: a displacement, split, or collapse of the polar vortex that increases stratospheric temperatures over the pole by 40 °C or more in a matter of days (Andrews et al., 1987; Butler et al., 2015; Kidston et al., 2015; Labitzke & Kunze, 2009). SSWs occur roughly six times per decade in the Northern Hemisphere (Butler et al., 2015) but have an outsized impact on the stratosphere, as the resultant temperature and wind anomalies can take over a month to return to the background state (Limpasuvan et al., 2004). Surface precursors to SSWs have been identified that are consistent with the mechanism of upwards propagation of wavenumbers 1 and 2, including blocking (Quiroz, 1986; Andrews et al., 1987; Martius et al., 2009) and sea level pressure or geopotential height anomalies (Ambaum

& Hoskins, 2002; Garfinkel et al., 2010; Kolstad et al., 2010; Lehtonen & Karpechko, 2016; ?, ?). But the presence of these precursors does not consistently lead to SSWs (Martius et al., 2009), motivating recent work emphasizing the importance of the stratospheric state in addition to tropospheric wave activity in generating SSWs (Birner & Albers, 2017).

The mechanisms and consequences of *downwards* propagation between the polar stratosphere and the troposphere are not as well-established. The strongest line of evidence for a downwards influence appears in changes to the northern annular mode (NAM), which explains a large fraction of the variance in the extratropical circulation and is defined by the first empirical orthogonal function of wintertime geopotential height at a given pressure (Baldwin, 2001; Thompson & Wallace, 2001). Baldwin and Dunkerton (2001) used composites of 90-day low-pass filtered NAM anomalies following SSWs to identify what appeared to be a downwards propagation of the negative NAM phase from the stratosphere to the surface over the course of two to three weeks, a result which subsequent studies have successfully replicated (Mitchell et al., 2013; Sigmond et al., 2013; Hitchcock & Simpson, 2014), although Hitchcock and Simpson (2014) point out that the signal in the troposphere is marginal at the 95% level. The two phases of the NAM correspond to significant differences in storminess and cold air outbreaks (Marshall et al., 2001; Thompson & Wallace, 2001; Hurrell et al., 2003), implying that SSWs could influence surface weather by propagating a negative NAM phase to the surface (Scaife et al., 2005; Kidston et al., 2015; Lee et al., 2019). But the conclusion of downwards propagation is complicated by the results of Plumb and Semeniuk (2003), which demonstrated that the *appearance* of downwards propagation from the stratosphere can be achieved even when the anomaly at each level is in fact produced by an upward influence from the lower boundary.

Progressing from the impact of SSWs on the NAM to an impact on surface weather extremes has introduced additional uncertainty. The best agreement across studies identifies a warm surface air temperature anomaly over the Labrador Sea and cooling over northern Russia on the order of 1–3 K one to two months after an SSW (Thompson et al., 2002; Kolstad et al., 2010; Lehtonen & Karpechko, 2016; Ayarzagüena et al., 2020). However, there is little consensus on the temperature response over populated mid-latitude coastal areas, and even less that holds across multiple data sets or models and is statistically significant. Taking North America (away from the Labrador Sea) as an example, some studies have found an overall cold anomaly (Thompson et al., 2002), an increase in the number of cold days (Zhang et al., 2020; Thompson et al., 2002), or an increase in the area experiencing anomalously cold temperatures (Yu et al., 2018) following SSWs, while others find no significant signal or disagreement across models and with reanalysis (Lehtonen & Karpechko, 2016; Ayarzagüena et al., 2020). The implications for surface weather are further complicated by the possibility of multiple sub-types of SSWs with distinct surface responses, which are washed out in the average. For example, Mitchell et al. (2013) found that displacement SSWs, in which the vortex is shifted off the pole, have a distinct surface temperature response from split SSWs, in which the vortex divides into two smaller vortices, but others have found little difference when separating by event type (Lehtonen & Karpechko, 2016; Charlton & Polvani, 2007; White et al., 2020). The sensitivity to the design of each study could indicate that the surface signal is too weak or varies widely from one SSW to another, in which case it may be of little interest for extreme weather prediction. But it could also mean that the time window or SSW sub-type classifications used so far are not a good representation of the important dynamics, in which case an analysis method that does not presuppose either a specific time lag or stratospheric dynamical feature is desirable, such as the one we will pursue below.

Looking ahead towards the end of the 21st century, there remains much uncertainty regarding the role that climate change will have in both upward and downward propagation. Some GCMs predict more frequent SSWs in the future (Kim et al., 2017; Schi-

manke et al., 2013; Bell et al., 2010; Charlton-Perez et al., 2008), but these results are not conclusive and often vary across models (Butchart et al., 2000; McLandress & Shepherd, 2009; Mitchell et al., 2012; Ayarzagüena et al., 2018, 2020; Rao & Garfinkel, 2021). There is already a large natural variability between different SSWs, making it more difficult to identify a robust trend. It has been suggested, for example, that the expected strengthening of the MJO would lead to forced planetary waves that may result in more frequent SSWs (Kang & Tziperman, 2017). Changes to sea ice and snow cover consistent with global warming have been associated with an observed increase in stratospheric polar vortex stretching events (Cohen et al., 2021), which are distinct from SSWs but have also been linked to cold spells over North America (Kretschmer, Cohen, et al., 2018), as well as an increased likelihood that SSWs will result in cold anomalies over Canada and the midwestern US (Zhang et al., 2020). But a recent study of 12 CMIP6 models under a $4\times CO_2$ experiment found no significant changes in the sea level pressure response to SSWs in most models (Ayarzagüena et al., 2020). In a much warmer climate, the negative NAM signal may become decoupled from SSWs altogether, as Hamouda et al. (2021) found that the negative Arctic Oscillation index (equivalent to NAM) following SSWs no longer propagates below the tropopause by the year 2300 under a high-emission scenario.

A variety of statistical analysis methods have been employed in the search for a robust signal of downwards propagation from stratospheric vortex disruptions to surface weather. Composites over many SSWs of the NAM index (Baldwin & Dunkerton, 2001; Mitchell et al., 2013; Hitchcock & Simpson, 2014; White et al., 2020) or surface temperature anomalies (Thompson et al., 2002; Kolstad et al., 2010; Lehtonen & Karpechko, 2016; Ayarzagüena et al., 2020) are widely used. But the NAM is a hemisphere-scale feature that does not necessarily translate to consistent weather extremes in any particular region, as demonstrated above. Composites over SSWs also rely on type and sub-type classifications that vary across studies (Butler et al., 2015), which can lead to conflicting conclusions about the existence or pattern of a surface weather response (?, ?). Clustering can identify dominant patterns within the stratosphere (Kretschmer, Coumou, et al., 2018; Kretschmer, Cohen, et al., 2018), but links to a surface response rely on compositing rather than a direct analysis of the covariance between surface and stratosphere. Additionally, while a time lag may be applied between the stratospheric cluster and the surface, there is no obvious way to identify the optimal time lag that maximizes the covariance between the stratospheric and tropospheric fields.

We attempt to identify teleconnections between the stratosphere and the surface in winter using Maximum Covariance Analysis (MCA). MCA allows us to identify rather than impose the time scales and spatial patterns most relevant to the covariance between tropospheric and stratospheric fields. We consider all combinations of three stratospheric fields (potential vorticity, zonal wind, and vertical Eliassen-Palm flux) and three tropospheric fields (daily minimum temperature, sea level pressure, and 500 hPa geopotential height) from over 60 years of the ERA5 reanalysis product in winter. We introduce a variable time lag that offsets the stratospheric and surface fields by up to ± 7 weeks to find the optimal lag representing the teleconnection time scale. MCA can then identify the tropospheric and stratospheric patterns that dominate the covariance between the two fields at that optimal lag.

We find evidence consistent with the upwards branch of stratosphere-troposphere teleconnections, with maximal covariance when the surface precedes the 10 hPa level by one week. However, we find no such evidence of downwards propagation. The surface pattern that accounts for the lion's share of the covariance with the stratosphere is neither the North Atlantic Oscillation nor the Northern Annular Mode.

2 Data & Methods

We use the ERA5 reanalysis product from 1959 to 2020 to investigate the covariance between stratospheric and tropospheric fields during Northern Hemisphere winter. On single levels, our fields include the 500 hPa geopotential height $Z500$, sea level pressure SLP, and the daily minimum surface air temperature $T_{\min}$. On pressure levels, we use Ertel potential vorticity PV, zonal wind U, and the vertical component of the Eliassen-Palm flux EP_p in pressure coordinates, which is calculated as follows,

$$EP_p = \frac{1}{d\bar{\theta}/dp} f a \cos\phi \, \overline{v'\theta'}, \tag{1}$$

where the overbar denotes a zonal average, f is the Coriolis parameter, a is the radius of the Earth, ϕ is latitude, $d\bar{\theta}/dp$ is the vertical derivative in pressure of the zonally-averaged potential temperature $\bar{\theta}$ calculated from daily output, and $\overline{v'\theta'}$ is the zonal average of the meridional wind anomaly $v' = v - \overline{v}$ multiplied by the potential temperature anomaly $\theta' = \theta - \overline{\theta}$.The variables v and θ are based on 6-hourly output and used in (1), after which EP_p is averaged over each day to produce daily means. All other fields are daily means calculated from hourly output except for surface temperature (daily minimums from hourly output). All fields were retrieved at $1^\circ \times 1^\circ$ resolution from 40°N to 90°N.

We process the data before calculating the covariance as follows. To account for the grid cell area represented by each grid point, we multiply each data field by $\cos\phi$ (for latitude-longitude fields, where ϕ is latitude) or by $\sqrt{\cos\phi}$ (for zonally-averaged fields like EP_p). At each point, we remove the linear trend and the mean over the entire time span from Jan 1959 through Dec 2020. We then calculate the seasonal cycle as the day-of-year mean at each grid point, smooth the day-of-year means with a 7-day Savitzky-Golay filter of polynomial order 1 (Savitzky & Golay, 1964), and subtract this smoothed seasonal cycle to convert each data field into an anomaly field.

We introduce a time lag between the tropospheric and stratospheric fields before calculating the covariance and repeat the analysis for different lags. The analysis centers on December–January, so at a time lag of zero both the tropospheric and stratospheric anomaly fields are composed of DJF for each year in the reanalysis. To introduce a time lag of n days (positive n when troposphere lags stratosphere, negative n for troposphere leads stratosphere, for $|n|$ up to 5 weeks), we consider the stratospheric field from $n/2$ days before Dec 1 through $n/2$ days before Feb 28, and conversely the tropospheric field from $n/2$ days after Dec 1 through $n/2$ days after Feb 28. In this way, a timeseries at any given point in the stratosphere is always n days before (or after, for negative n) a corresponding timeseries at any given point in the troposphere. This method maximizes the amount of time spent in DJF across both fields and allows for a variable time lag of any length and either direction in time.

To identify the relevant teleconnection time scales, we calculate the total squared covariance as a function of the time lag between a stratospheric field and a tropospheric field (Perlwitz & Harnik, 2003, 2004). We start with a stratospheric anomaly field X, given at M grid points and N daily values and arranged in an $M \times N$ matrix, and a tropospheric field Y, an $L \times N$ matrix, where each column of a matrix corresponds to the spatial field on a particular day written as a vector. The covariance matrix is then,

$$C = \frac{XY^T}{N}. \tag{2}$$

Each element of C, c_{ij}, is then the covariance over the entire timeseries between location i in X and location j in Y. The total squared covariance between the two fields is $\sum_{i,j} c_{ij}^2$ and can be compared across time lags to determine the time lag that maximizes the covariance between the two fields. Note that, while X and Y must match in the length of the time dimension N, they need not share a spatial dimension. For example, we can

calculate C when X is EP_p, which is solely a function of latitude, and Y is sea level pressure, which is a function of both latitude and longitude.

To identify the patterns in the stratosphere and the surface that best explain the covariance between the two, we apply Maximum Covariance Analysis (MCA). MCA identifies a series of pairs of patterns (modes) of the two fields that have the maximum covariance over the data time series (Bretherton et al., 1992). To apply MCA, we use singular value decomposition on the covariance matrix C,

$$C = U\Sigma V^T. \tag{3}$$

This identifies a series of mutually orthogonal modes, each characterized by a pattern in the X field (columns of U) and a corresponding pattern in the Y field (columns of V). The column vectors $\mathbf{u}_1$ and $\mathbf{v}_1$, for example, the first column of each matrix, are the most highly correlated patterns between the two fields. The fraction of the total covariance between the two fields that is explained by a given mode can be determined using the corresponding singular value in the diagonal matrix Σ. Thus the first mode explains the largest fraction, $\sigma_1^2 / \sum_k \sigma_k^2$, of the covariance between X and Y and each subsequent mode explains a progressively smaller fraction.

3 Results

XX an introduction paragraph outlining the results section

3.1 A Demonstration of MCA for Troposphere-Stratosphere Teleconnections

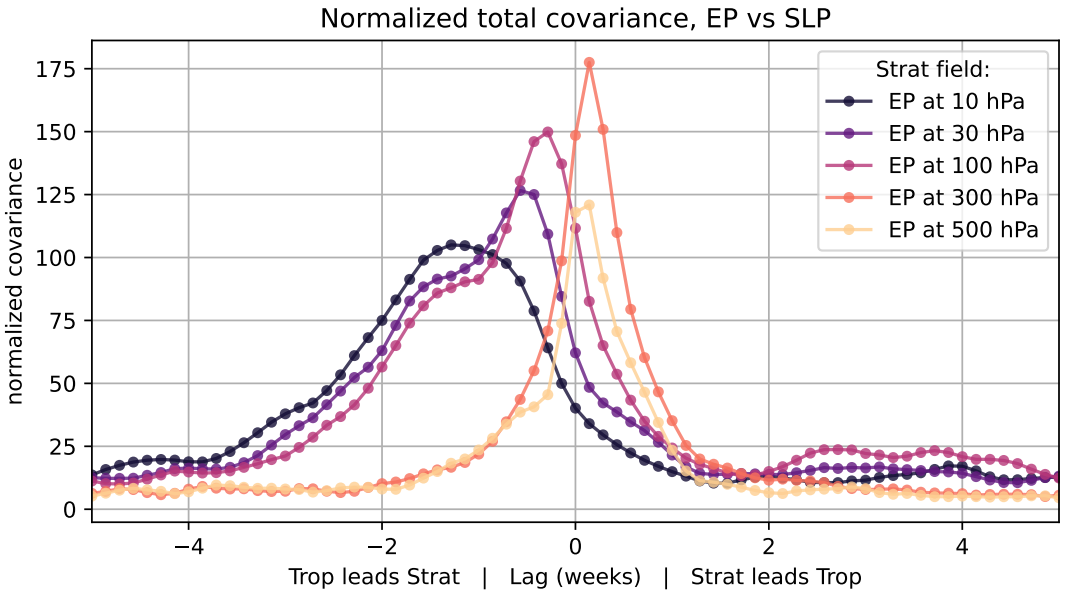

Figure 1. Peaks in total squared covariance pick out timescales of covariance. The total squared covariance is shown between sea level pressure (SLP) and the vertical component of Eliassen-Palm flux at multiple pressure levels (EP) as a function of the time lag between the surface and the stratosphere. Each curve is normalized by XXX.

To identify the time scale of teleconnections between the wintertime stratosphere and troposphere, we first demonstrate that the total squared covariance as a function

of lag is a suitable tool to pick out those time scales. Sea level pressure anomalies have been shown to precede major disruptions of the stratospheric polar vortex (?, ?). The vertical component of Eliassen-Palm (EP) flux is know to be a useful diagnostic for upwards wave propagation (?, ?). We therefore begin by confirming the covariance between the two in Figure 1. For EP fluxes in the stratosphere (10, 30, and 100 hPa), sea level pressure tends to lead EP flux by 2–9 days, while there is negligible lead or lag between SLP and EP fluxes in the troposphere (300 and 500 hPa). Both the lag and magnitude of maximal covariance also shifts in a way that is consistent with upwards propagation: the longest optimal lag and smallest maximal covariance occurs between the surface and 10 hPa, which are the furthest apart in space, and the lag shortens even as the covariance grows as we consider EP fluxes closer to the surface. EP flux at 500 hPa is an exception, as its covariance with the surface is smaller than at 300 hPa, but this could be due to increased noise from synoptic activity.

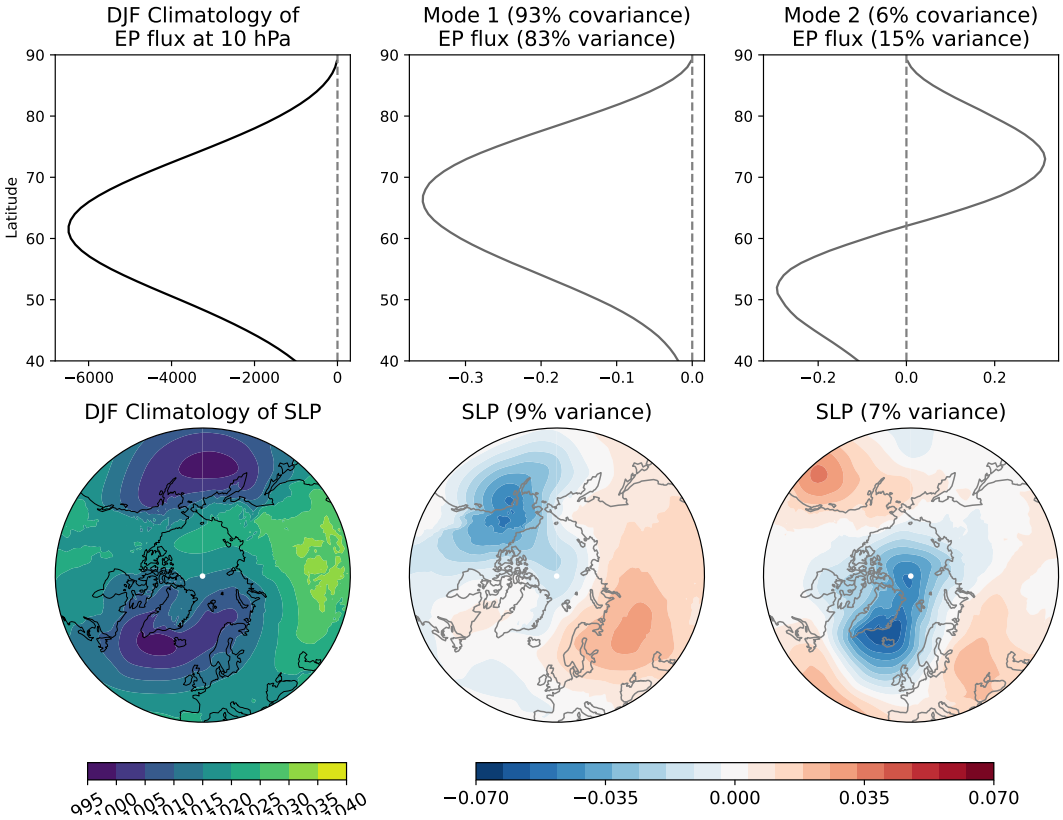

Figure 2. MCA identifies a known mode of covariance between the surface and stratosphere. The climatology and first two MCA modes are shown for EP at 10 hPa (stratosphere) and sea level pressure (surface) at a time lag of −9 days (surface precedes stratosphere), corresponding to the maximum total covariance in Figure 1. The percent of total covariance explained by each mode is shown in parentheses at the top, while the percent of variance in a specific field explained by the corresponding pattern from that mode is shown above each subplot. Note that a negative EP flux is directed upwards in the pressure coordinates used here.

We follow up with MCA to identify the spatial patterns at the surface and in the stratosphere responsible for the covariance during upwards propagation. Figure 2 shows the first two modes produced by MCA between the sea level pressure and EP at 10 hPa with a time lag of −9 days, the optimal lag corresponding to the largest covariance be-

tween these two fields in Figure 1. Mode 1 corresponds to a strengthening and slight northward shift of the climatological peak in EP flux centered at 65°N (Fig. 2b) and a sea level pressure dipole with one pole over Alaska and the other over Western Russia (Fig. 2e). The sea level pressure pattern of mode 1 is consistent with a documented precursor to SSWs (Kolstad et al., 2010; Lehtonen & Karpechko, 2016; ?, ?), with a low over Alaska and the North Pacific and a high over Western Russia, which increases our confidence that MCA is able to capture established modes of covariability between the surface and the stratosphere.

Mode 1 accounts for the overwhelming majority, 93%, of the covariance between sea level pressure and vertical EP flux at 10 hPa. But while the stratospheric part of this mode also corresponds to the lion's share of the variance within EP flux at 10 hPa (83%), the surface component accounts for only 9% of the variance in the surface. We can conclude that the sea level pressure precursor described by mode 1 is relatively rare but corresponds to a strengthening of the EP10 peak at 65°N that accounts for most of the variability in the stratosphere. Mode 2, which accounts for only 6% of the covariance between sea level pressure and EP10, corresponds to a north/south shift of the EP10 maximum and resembles the Northern Annular Mode (NAM) or North Atlantic Oscillation at the surface (?, ?; Hamouda et al., 2021) with poles over the Icelandic Low and the North Atlantic (Fig. 2c, f). This is somewhat surprising; the strength of the NAM index has long been considered both a precursor to (?, ?) and consequence of (?, ?) SSWs, but in our analysis the NAM-like pattern accounts for only 6% of the covariance between surface and stratosphere while a different pattern (Fig. 2e) accounts for almost all of the covariance between them.

3.2 Characterizing upwards vs downwards influence

In expanding our analysis to a wide variety of both stratospheric and tropospheric fields, we find that lags from a few days up to one week maximize the total covariance in almost all cases. We consider several stratospheric fields at 10 hPa, including potential vorticity (PV), zonal wind (U) and the vertical component of EP flux (EP), alongside several tropospheric fields including daily minimum surface temperature (T_{min}), sea level pressure (SLP), and the 500 hPa geopotential height (Z500). Figure 3 of the total covariance between stratospheric fields PV10, U10, and EP10 and tropospheric fields T_{min}, SLP, and Z500 shows maximum total covariance at negative lags and insignificant covariance at positive lags for almost all pairs of tropospheric and stratospheric fields. Naively, one would expect upwards propagation to result in a peak at negative lags (troposphere leads stratosphere) and downwards propagation to result in a peak at positive lags (troposphere lags stratosphere). These results, therefore, provide support for upwards but not downwards propagation.

The singular exception is U10 and sea level pressure, which has a secondary peak when the surface lags the stratosphere by +3 days (Figure 3b). Previous studies have identified downward propagation of zonal-mean zonal wind anomalies in the wintertime stratosphere (?, ?, ?), but over longer timescales of weeks to months, and not in the zonally-resolved wind field we have used here.

Much of the interest in downwards propagation in the literature is concerned with the response of temperature extremes to stratospheric disruption, as such a connection could be used to improve weather prediction lead times. However, we find little indication of a downwards influence between any of our stratospheric fields and the daily minimum temperature T_{min}. Instead, T_{min} tends to lead all stratospheric fields by a few days, but the dynamical mechanism is more likely that sea level pressure, which has the largest lead time of any tropospheric field considered, is related to upwards propagation while T_{min} appears to respond to the surface pressure anomalies a few days later. Indeed, we find that the pattern of T_{min} for mode 1 (not shown) is consistent with the geostrophic

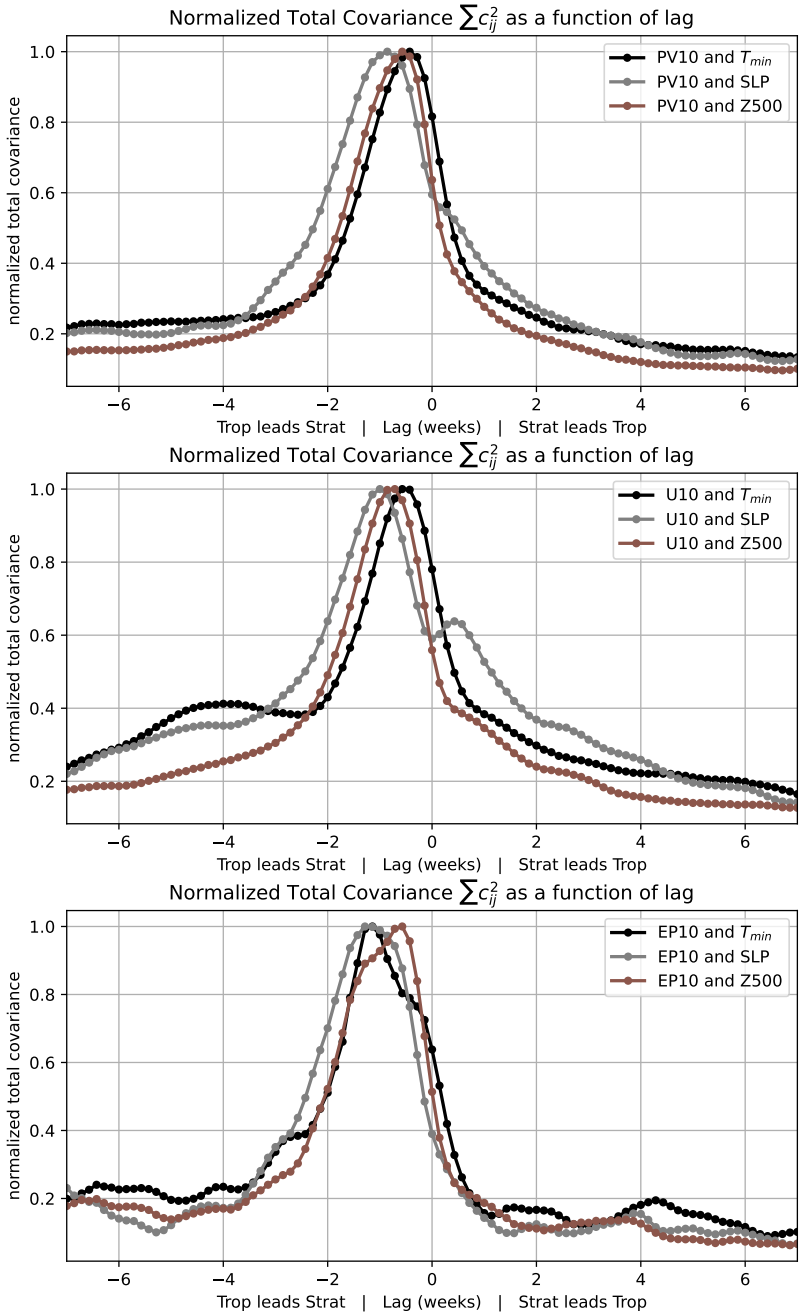

Figure 3. Covariance between different stratosphere-troposphere field pairs show evidence for upwards but not downwards propagation. Total covariance between a stratospheric field (PV (top), U (middle) or EP flux (bottom)) at 10 hPa and a tropospheric field (daily minimum surface temperature (black), sea level pressure (grey), or 500 hPa geopotential height (brown)) as a function of the lag in weeks between the two fields. Each curve is normalized to have a maximum of 1.

circulation anomalies that would be induced by the sea level pressure anomalies for mode 1, with northward (warm) advection over Canada and southward (cold) over eastern Russia (Figure supplementary-XX).

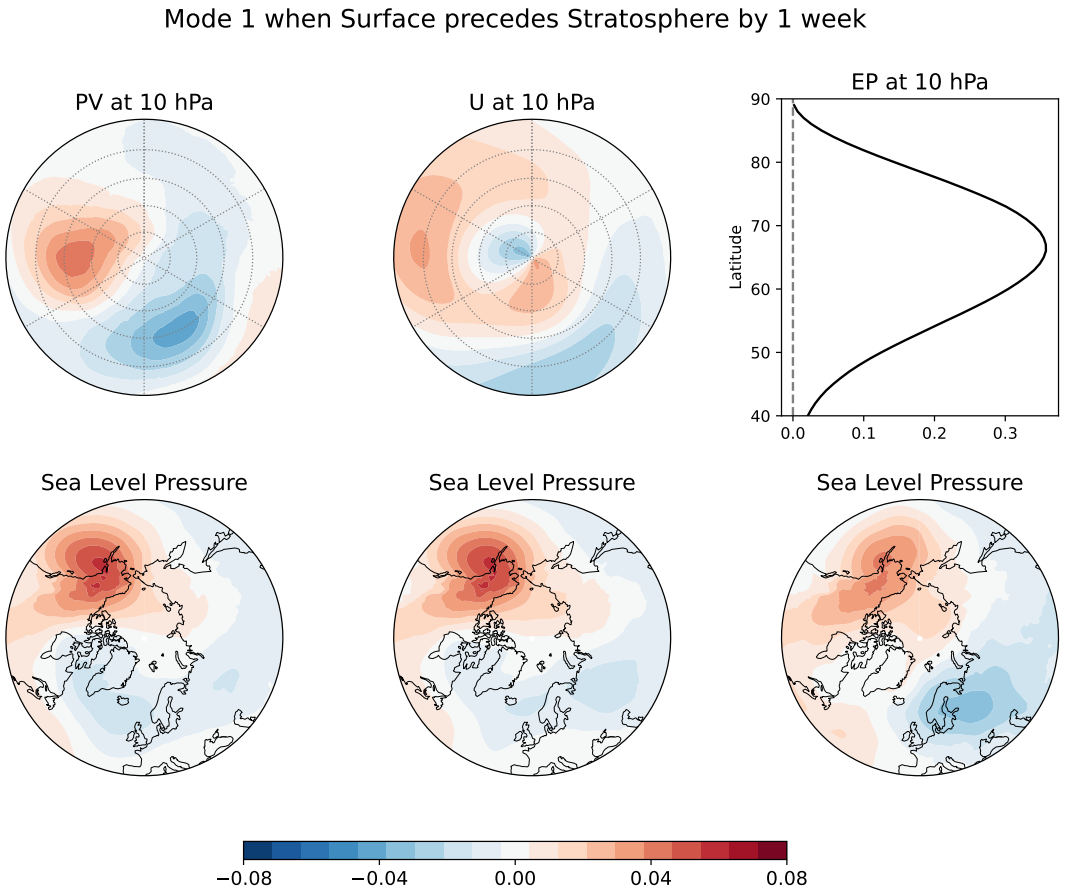

Figure 4. The sea level pressure anomaly that leads the stratosphere by one week later is similar across different stratospheric fields and is not either the NAO or NAM/AO. The first MCA mode is shown between a stratospheric field at 10 hPa (PV (left), U (middle), or EP flux (right)) and sea level pressure at a lag of −1 week. As is conventional, these MCA mode patterns are normalized to a vector norm of 1.

When we expand our consideration to the dominant mode across all stratospheric fields, the particular significance of the sea level pressure anomaly that we identified in Figure 2 is reinforced. Figure 4 shows the patterns corresponding to the first MCA mode across three different stratospheric fields at 10 hPa with a lag of −1 week. The sea level pressure pattern is nearly identical across all three stratospheric fields, with slight variations in the location of the pole over Eurasia. This mode indicates that a low pressure anomaly over Alaska and a high over western Russia at the surface tend to be followed a week later by: a shift of the stratospheric vortex into the sector over western Russia (4a); a clockwise circulation anomaly over western Russia and a counterclockwise anomaly over northwestern Canada in the stratosphere (4b); and a strengthening of the climatological peak in EP10 (4c). While there are previous studies that have identified this sea level pressure pattern as a precursor to SSWs (Kolstad et al., 2010; Lehtonen & Karpechko, 2016; ?, ?), there are others that have found a different pattern to be more prominent (Martius et al., 2009; Kolstad et al., 2010; Mitchell et al., 2013). As our MCA analysis

is not restricted to SSWs but instead considers covariance over the entire winter, one explanation for this disagreement is that the sea level pressure precursor we and others have identified is not limited to SSWs but instead describes a more general mode of covariability between the surface and the stratosphere.

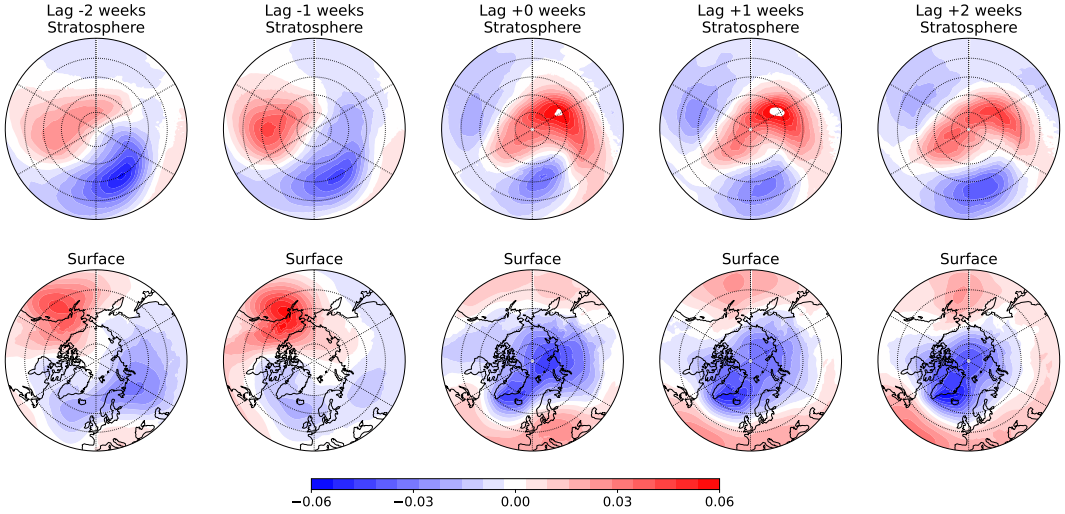

Figure 5. The structure of mode 1 changes near lag zero. The mode 1 pattern that maximizes covariance between PV at 10 hPa (upper row) and the sea level pressure (lower) is shown for five different lags ranging from −2 weeks to +2 weeks.

We can also consider how the first mode itself changes as a function of lag between the tropospheric field (SLP) and stratospheric (PV), illustrated in Figure 5. A major shift occurs between a lag of −1 week and no lag: the dominant mode we identified in Figure 4 subsides and is replaced by a pattern much more reminiscent of the NAM in sea level pressure. This NAM-like mode also persists over a large range of lags; the sea level pressure pattern that most closely covaries with PV10 at no lag also tends to lag it by +1 and even +2 weeks.

(XX expand here) Alternative to downwards propagation. The persistence of the mode 1 pattern as a function of lag likely reflects a persistence of the corresponding dynamical feature. Since the total squared covariance decreases as the lag increases from zero (Figure 3a), it is likely that the stratospheric and surface patterns that make up the dominant mode at a lag of zero tend to co-occur in time and then linger for a few weeks, such that the same pattern is still the dominant mode even at large lags when the covariance itself is small. Our identification of a NAM-like pattern at the surface for positive lags is consistent with other studies that have found that a negative NAM signal at the surface tends to follow SSWs in observations (?, ?) and models (?, ?). We further note that the PV anomaly of mode 1 at positive lags is consistent with a split-type SSW, placing daughter vortices over Northern Europe and western Canada, which was found by CITET(Mitchell et al., 2013) to lead to a negative NAM signal at the surface where displacement-type SSWs did not.

3.3 The Search for Downwards Propagation: Downwards EP flux

The lack of evidence for a downwards propagation signal in the above analysis leads us to attempt to separate upwards from downwards EP prior to calculating the covariance. [Explain masking method here: discuss positive vs negative anomalies, also the caveats

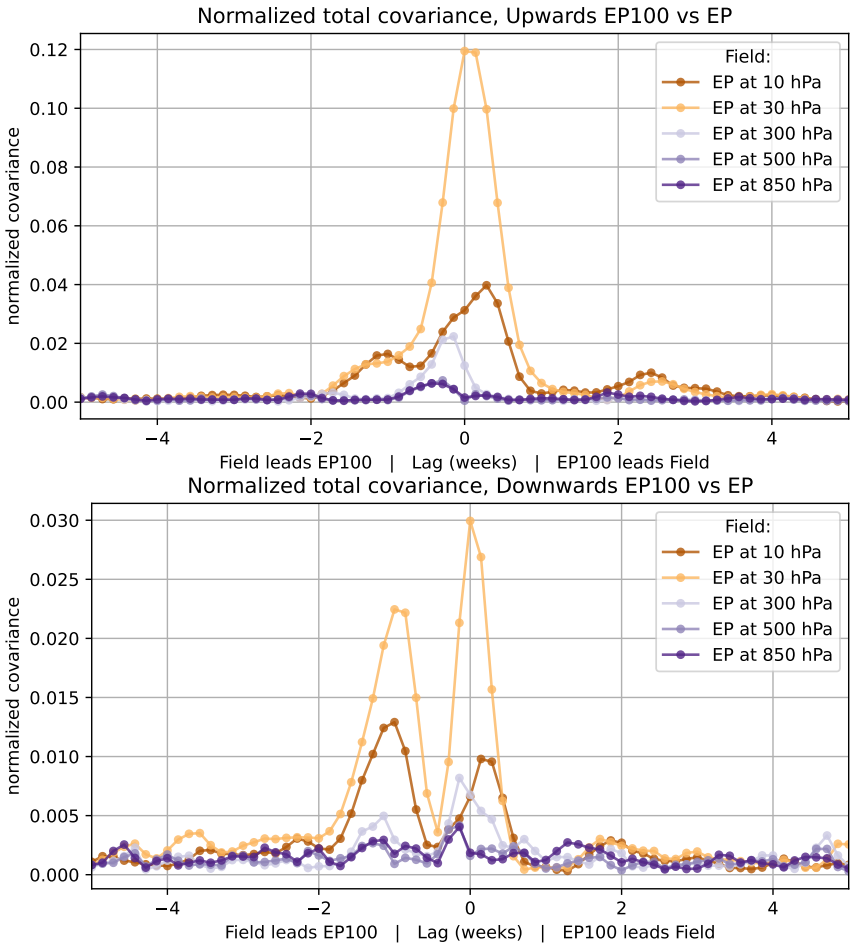

Figure 6. It is feasible to track upwards but not downwards propagation with positive and negative EP flux anomalies. Total covariance between "upwards" (negative EP flux anomaly over 2 standard deviations) or "downwards" (positive anomaly) EP flux at 100 hPa and total EP flux at various levels throughout the troposphere and stratosphere. Brown lines correspond to levels above EP100 while purple indicates levels below EP100. Each curve is normalized by XXX.

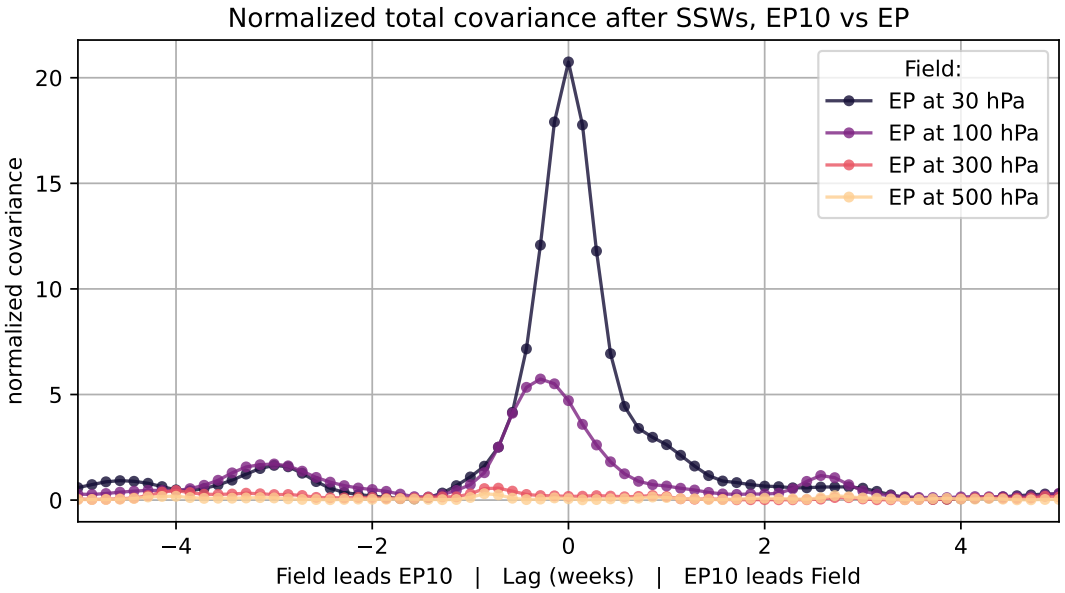

Figure 7. Downwards propagation still not visible when restricting to the 6-week period following SSWs

that this isn't exactly upward vs downward etc; reason we aren't masking both levels is because there are so few data points left that the plots become just noise].

Figure 6 shows the covariance between positive-anomaly or negative-anomaly EP at 100 hPa and the total EP at levels both above and below. There is evidence of upwards propagation in Figure 6a: EP below 100 hPa tends to lead that level (brown lines peak at positive lags) while EP above 100 hPa tends to lag (purple lines peak at negative lags). The magnitude of maximum covariance varies with the vertical separation between the two fields (paler shades have higher magnitude than darker shades). Noting that the peak for EP at 850 hPa occurs about 5 days before the peak for 10 hPa, one might conclude that it takes about 5 days for upwards EP flux anomalies to be communicated between 850 and 10 hPa. [XX discussion of a reference]

Downwards propagation is not as evident in Figure 6b. For downwards propagation, we would expect each curve to peak in the reverse order with respect to lag that they did for upwards EP: 10 and 30 hPa would peak at negative lags and 300, 500 and 850 hPa at positive lags. Instead, there are peaks at both positive and negative lags for 10, 30, and 300 hPa while 500 and 850 hPa have no peaks distinguishable from the noise. This difficulty highlights a limitation of the vertical component of EP flux anomalies: we are unable to distinguish between, for example, a weakening of upwards EP flux and the presence of downwards EP flux. The conflation of the two may help explain the presence of peaks at both positive and negative lags in Figure 6b. The upwards EP flux signal is likely cleaner than the downwards because upwards wave propagation dominates the time series. [SUMMARIZE: a valiant attempt, but maybe another method would work better]

3.4 The Search for Downwards Propagation: Composites of SSWs

TO BE WRITTEN

3.5 The Search for Downwards Propagation: EP Following SSWs

Rather than incorporate all winter days into our analysis, we now restrict our analysis to only those times corresponding to SSWs and look for downwards propagation in these better-studied periods. We first identify all major SSWs between 1959 and 2020 in the ERA5 dataset using the zonal-mean zonal wind at 60°N criterion of CITET(Charlton & Polvani, 2007). For each SSW, we restrict the stratospheric field to the 6 weeks following SSW onset, then apply a lag relative to that 6-week window to get a corresponding tropospheric time series. By combining these 6-week windows for all SSWs, we produce new timeseries that can be used to calculate the total covariance between the troposphere and stratosphere focused on the period during and after SSWs. Note that the same processing was applied to each data set before selecting out the SSWs as was described in section 2: at each grid point, apply area-weighting, remove the linear trend, and subtract off the seasonal cycle. For reference, we perform the same analysis but using the 6 weeks preceding SSW onset.

Even restricted to the period following SSWs, for which the magnitude of the disruption to the stratospheric vortex gives the best reason to expect downwards propagation, there is still negligible covariance between stratospheric and tropospheric fields. Figure 7 shows the total squared covariance between the EP flux at 10 hPa in the 6 weeks following SSWs and EP flux at lower levels. The covariance is only significant within the stratosphere, and even there the lower levels tend to lead rather than lag EP10.

4 Conclusions

We set out to identify time lags and spatial patterns most relevant to covariance between the troposphere and stratosphere in Northern Hemisphere winter. We consider the total covariance as a function of time lag between a set of tropospheric and stratospheric fields to identify the optimal time lag and search for signals of upwards and downwards propagation. We find that, while there is evidence of an upwards influence with a time lag of about one week, there is no evidence of a downwards influence. This was determined using daily ERA5 output of Ertel potential vorticity, zonal wind, and the vertical component of EP flux at various pressure levels to represent the stratosphere and daily minimum surface temperature, sea level pressure, and the 500 hPa geopotential height to represent the troposphere. The covariance between the two fields was maximized, for all pairs of fields, when the troposphere leads the 10 hPa level by up to one week (with a shorter lag for lower stratospheric fields). At a given time lag, we employed Maximum Covariance Analysis to identify the spatial patterns that account for the covariance between the two fields, with which we were able to identify a sea level pressure pattern that accounts for the majority of the time-lagged covariance with all three stratospheric fields, featuring a pressure anomaly over Alaska and another of the opposite sign over western Russia.

Acknowledgments

This work was funded by the U.S. Department of Energy (DOE) Office of Science Biological and Environmental Research grant DE-SC0023134. ET thanks the Weizmann Institute for its hospitality during parts of this work.

References

Ambaum, M. H. P., & Hoskins, B. J. (2002). The NAO Troposphere–Stratosphere Connection. *Journal of Climate*, *15*(14), 1969–1978.

Andrews, D., Holton, J., & Leovy, C. (1987). *Middle atmosphere dynamics*. Academic Press.

Ayarzagüena, B., Charlton-Perez, A. J., Butler, A. H., Hitchcock, P., Simpson, I. R.,

Polvani, L. M., ... Watanabe, S. (2020). Uncertainty in the Response of Sudden Stratospheric Warmings and Stratosphere-Troposphere Coupling to Quadrupled CO2 Concentrations in CMIP6 Models. *Journal of Geophysical Research: Atmospheres*, *125*(6), e2019JD032345. doi: 10.1029/2019JD032345

Ayarzagüena, B., Polvani, L. M., Langematz, U., Akiyoshi, H., Bekki, S., Butchart, N., ... Zeng, G. (2018, August). No robust evidence of future changes in major stratospheric sudden warmings: a multi-model assessment from CCMI. *Atmospheric Chemistry and Physics*, *18*(15), 11277–11287. doi: 10.5194/acp-18-11277-2018

Baldwin, M. P. (2001). Annular modes in global daily surface pressure. *Geophysical Research Letters*, *28*(21), 4115–4118. doi: 10.1029/2001GL013564

Baldwin, M. P., Ayarzagüena, B., Birner, T., Butchart, N., Butler, A. H., Charlton-Perez, A. J., ... Pedatella, N. M. (2021). Sudden Stratospheric Warmings. *Reviews of Geophysics*, *59*(1), e2020RG000708. doi: 10.1029/2020RG000708

Baldwin, M. P., & Dunkerton, T. J. (2001, October). Stratospheric harbingers of anomalous weather regimes. *Science*, *294*(5542), 581–4.

Bell, C. J., Gray, L. J., & Kettleborough, J. (2010, July). Changes in Northern Hemisphere stratospheric variability under increased CO_2 concentrations. *Quarterly Journal of the Royal Meteorological Society*, *136*(650), 1181-1190. doi: 10.1002/qj.633

Birner, T., & Albers, J. R. (2017). Sudden Stratospheric Warmings and Anomalous Upward Wave Activity Flux. *Sola*, *13A*(Special_Edition), 8–12. doi: 10.2151/sola.13A-002

Bretherton, C. S., Smith, C., & Wallace, J. M. (1992, June). An Intercomparison of Methods for Finding Coupled Patterns in Climate Data. *Journal of Climate*, *5*(6), 541–560. doi: 10.1175/1520-0442(1992)005⟨0541:AIOMFF⟩2.0.CO;2

Butchart, N., Austin, J., Knight, J. R., Scaife, A. A., & Gallani, M. L. (2000, July). The response of the stratospheric climate to projected changes in the concentrations of well-mixed greenhouse gases from 1992 to 2051. *Journal of Climate*, *13*(13), 2142–2159. doi: 10.1175/1520-0442(2000)013⟨2142:TROTSC⟩2.0.CO;2

Butler, A. H., Seidel, D. J., Hardiman, S. C., Butchart, N., Birner, T., & Match, A. (2015, November). Defining Sudden Stratospheric Warmings. *Bulletin of the American Meteorological Society*, *96*(11), 1913–1928. doi: 10.1175/BAMS-D-13-00173.1

Charlton, A. J., & Polvani, L. M. (2007, February). A New Look at Stratospheric Sudden Warmings. Part I: Climatology and Modeling Benchmarks. *Journal of Climate*, *20*(3), 449–469. doi: 10.1175/JCLI3996.1

Charlton-Perez, A. J., Polvani, L. M., Austin, J., & Li, F. (2008, August). The frequency and dynamics of stratospheric sudden warmings in the 21st century. *Journal of Geophysical Research*, *113*(D16), D16116. doi: 10.1029/2007JD009571

Charney, J. G., & Drazin, P. G. (1961). Propagation of planetary-scale disturbances from the lower into the upper atmosphere. *Journal of Geophysical Research (1896-1977)*, *66*(1), 83–109. doi: 10.1029/JZ066i001p00083

Cohen, J., Agel, L., Barlow, M., Garfinkel, C. I., & White, I. (2021, September). Linking Arctic variability and change with extreme winter weather in the United States. *Science*, *373*(6559), 1116–1121. doi: 10.1126/science.abi9167

Garfinkel, C. I., Hartmann, D. L., & Sassi, F. (2010, June). Tropospheric Precursors of Anomalous Northern Hemisphere Stratospheric Polar Vortices. *Journal of Climate*, *23*(12), 3282–3299. doi: 10.1175/2010JCLI3010.1

Hamouda, M. E., Pasquero, C., & Tziperman, E. (2021, February). Decoupling of the Arctic Oscillation and North Atlantic Oscillation in a warmer climate. *Nature Climate Change*, *11*(2), 137–142. doi: 10.1038/s41558-020-00966-8

Hitchcock, P., & Simpson, I. R. (2014, October). The Downward Influence of Strato-

spheric Sudden Warmings. *Journal of the Atmospheric Sciences*, *71*(10), 3856–3876. doi: 10.1175/JAS-D-14-0012.1

Hurrell, J. W., Kushnir, Y., Ottersen, G., & Visbeck, M. (2003). An overview of the North Atlantic Oscillation. In J. W. Hurrell, Y. Kushnir, G. Ottersen, & M. Visbeck (Eds.), *Geophysical Monograph Series* (Vol. 134, pp. 1–35). Washington, D. C.: American Geophysical Union. doi: 10.1029/134GM01

Kang, W., & Tziperman, E. (2017, November). More Frequent Sudden Stratospheric Warming Events due to Enhanced MJO Forcing Expected in a Warmer Climate. *Journal of Climate*, *30*(21), 8727–8743. doi: 10.1175/JCLI-D-17-0044.1

Kidston, J., Scaife, A. A., Hardiman, S. C., Mitchell, D. M., Butchart, N., Baldwin, M. P., & Gray, L. J. (2015, June). Stratospheric influence on tropospheric jet streams, storm tracks and surface weather. *Nature Geoscience*, *8*(6), 433–440. doi: 10.1038/ngeo2424

Kim, J., Son, S.-W., Gerber, E. P., & Park, H.-S. (2017, July). Defining Sudden Stratospheric Warming in Climate Models: Accounting for Biases in Model Climatologies. *Journal of Climate*, *30*(14), 5529–5546. doi: 10.1175/JCLI-D-16-0465.1

Kolstad, E. W., Breiteig, T., & Scaife, A. A. (2010). The association between stratospheric weak polar vortex events and cold air outbreaks in the Northern Hemisphere. *Quarterly Journal of the Royal Meteorological Society*, *136*(649), 886–893. doi: 10.1002/qj.620

Kretschmer, M., Cohen, J., Matthias, V., Runge, J., & Coumou, D. (2018, November). The different stratospheric influence on cold-extremes in Eurasia and North America. *npj Climate and Atmospheric Science*, *1*(1), 1–10. doi: 10.1038/s41612-018-0054-4

Kretschmer, M., Coumou, D., Agel, L., Barlow, M., Tziperman, E., & Cohen, J. (2018, January). More-Persistent Weak Stratospheric Polar Vortex States Linked to Cold Extremes. *Bulletin of the American Meteorological Society*, *99*(1), 49–60. doi: 10.1175/BAMS-D-16-0259.1

Labitzke, K., & Kunze, M. (2009). On the remarkable Arctic winter in 2008/2009. *Journal of Geophysical Research: Atmospheres*, *114*(D1). doi: 10.1029/2009JD012273

Lee, S. H., Furtado, J. C., & Charlton-Perez, A. J. (2019). Wintertime North American Weather Regimes and the Arctic Stratospheric Polar Vortex. *Geophysical Research Letters*, *46*(24), 14892–14900. doi: 10.1029/2019GL085592

Lehtonen, I., & Karpechko, A. Y. (2016). Observed and modeled tropospheric cold anomalies associated with sudden stratospheric warmings. *Journal of Geophysical Research: Atmospheres*, *121*(4), 1591–1610. doi: 10.1002/2015JD023860

Limpasuvan, V., Thompson, D. W. J., & Hartmann, D. L. (2004, July). The Life Cycle of the Northern Hemisphere Sudden Stratospheric Warmings. *Journal of Climate*, *17*(13), 2584–2596. doi: 10.1175/1520-0442(2004)017⟨2584:TLCOTN⟩2.0.CO;2

Marshall, J., Kushnir, Y., Battisti, D., Chang, P., Czaja, A., Dickson, R., ... Visbeck, M. (2001). North Atlantic climate variability: phenomena, impacts and mechanisms. *International Journal of Climatology*, *21*(15), 1863–1898. doi: 10.1002/joc.693

Martius, O., Polvani, L. M., & Davies, H. C. (2009). Blocking precursors to stratospheric sudden warming events. *Geophysical Research Letters*, *36*(14). doi: 10.1029/2009GL038776

Matsuno, T. (1971, November). A Dynamical Model of the Stratospheric Sudden Warming. *Journal of the Atmospheric Sciences*, *28*(8), 1479–1494. doi: 10.1175/1520-0469(1971)028⟨1479:ADMOTS⟩2.0.CO;2

McIntyre, M. E., & Palmer, T. N. (1984, September). The 'surf zone' in the stratosphere. *Journal of Atmospheric and Terrestrial Physics*, *46*(9), 825–849. doi: 10.1016/0021-9169(84)90063-1

McLandress, C., & Shepherd, T. G. (2009, October). Impact of climate change on stratospheric sudden warmings as simulated by the Canadian middle atmosphere model. *Journal of Climate*, *22*(20), 5449–5463. doi: 10.1175/2009JCLI3069.1

Mitchell, D. M., Gray, L. J., Anstey, J., Baldwin, M. P., & Charlton-Perez, A. J. (2013, April). The Influence of Stratospheric Vortex Displacements and Splits on Surface Climate. *Journal of Climate*, *26*(8), 2668–2682. doi: 10.1175/JCLI-D-12-00030.1

Mitchell, D. M., Osprey, S. M., Gray, L. J., Butchart, N., Hardiman, S. C., Charlton-Perez, A. J., & Watson, P. (2012, August). The effect of climate change on the variability of the northern hemisphere stratospheric polar vortex. *Journal of the Atmospheric Sciences*, *69*(8), 2608–2618. doi: 10.1175/JAS-D-12-021.1

Perlwitz, J., & Harnik, N. (2003, September). Observational Evidence of a Stratospheric Influence on the Troposphere by Planetary Wave Reflection. *Journal of Climate*, *16*(18), 3011–3026. doi: 10.1175/1520-0442(2003)016⟨3011:OEOASI⟩2.0.CO;2

Perlwitz, J., & Harnik, N. (2004, December). Downward Coupling between the Stratosphere and Troposphere: The Relative Roles of Wave and Zonal Mean Processes. *Journal of Climate*, *17*(24), 4902–4909. doi: 10.1175/JCLI-3247.1

Plumb, R. A. (2010). Planetary Waves and the Extratropical Winter Stratosphere. *The Stratosphere: Dynamics, Transport, and Chemistry*, *190*, 23–41.

Plumb, R. A., & Semeniuk, K. (2003). Downward migration of extratropical zonal wind anomalies. *Journal of Geophysical Research: Atmospheres*, *108*(D7). doi: 10.1029/2002JD002773

Quiroz, R. S. (1986). The association of stratospheric warmings with tropospheric blocking. *Journal of Geophysical Research: Atmospheres*, *91*(D4), 5277–5285. doi: 10.1029/JD091iD04p05277

Rao, J., & Garfinkel, C. I. (2021, February). CMIP5/6 models project little change in the statistical characteristics of sudden stratospheric warmings in the 21st century. *Environmental Research Letters*, *16*(3), 034024. doi: 10.1088/1748-9326/abd4fe

Savitzky, A., & Golay, M. J. E. (1964, Jul). Smoothing and Differentiation of Data by Simplified Least Squares Procedures. *Analytical Chemistry*, *36*(8), 1627–1639. doi: 10.1021/ac60214a047

Scaife, A. A., Knight, J. R., Vallis, G. K., & Folland, C. K. (2005). A stratospheric influence on the winter NAO and North Atlantic surface climate. *Geophysical Research Letters*, *32*(18). doi: 10.1029/2005GL023226

Schimanke, S., Spangehl, T., Huebener, H., & Cubasch, U. (2013). Variability and trends of major stratospheric warmings in simulations under constant and increasing GHG concentrations. *Climate Dynamics*, *40*(7-8), 1733–1747. doi: 10.1007/s00382-012-1530-x

Sigmond, M., Scinocca, J. F., Kharin, V. V., & Shepherd, T. G. (2013, February). Enhanced seasonal forecast skill following stratospheric sudden warmings. *Nature Geoscience*, *6*(2), 98–102. doi: 10.1038/ngeo1698

Thompson, D. W. J., Baldwin, M. P., & Wallace, J. M. (2002, June). Stratospheric Connection to Northern Hemisphere Wintertime Weather: Implications for Prediction. *Journal of Climate*, *15*(12), 1421–1428. doi: 10.1175/1520-0442(2002)015⟨1421:SCTNHW⟩2.0.CO;2

Thompson, D. W. J., & Wallace, J. M. (2001, July). Regional climate impacts of the Northern Hemisphere annular mode. *Science*, *293*(5527), 85–9.

White, I. P., Garfinkel, C. I., Gerber, E. P., Jucker, M., Hitchcock, P., & Rao, J. (2020, July). The Generic Nature of the Tropospheric Response to Sudden Stratospheric Warmings. *Journal of Climate*, *33*(13), 5589–5610. doi: 10.1175/JCLI-D-19-0697.1

Yu, Y., Cai, M., Shi, C., & Ren, R. (2018, September). On the Linkage among Strong Stratospheric Mass Circulation, Stratospheric Sudden Warming, and Cold Weather Events. *Monthly Weather Review*, *146*(9), 2717–2739. doi: 10.1175/MWR-D-18-0110.1

Zhang, P., Wu, Y., Chen, G., & Yu, Y. (2020, November). North American cold events following sudden stratospheric warming in the presence of low Barents-Kara Sea sea ice. *Environmental Research Letters*, *15*(12), 124017. doi: 10.1088/1748-9326/abc215